Coarse-Grained Molecular Simulation of Penetrant Diffusion in a Glassy Polymer Using Reverse and Kinetic Monte Carlo

Michael L. Greenfield*,†

Department of Chemical Engineering, University of California, Berkeley, Berkeley, California 94720

Doros N. Theodorou

Department of Chemical Engineering, University of Patras and ICE/HT-FORTH, P.O. Box 1414, GR 26500 Patras, Greece

Received December 19, 2000; Revised Manuscript Received August 23, 2001

ABSTRACT: A coarse-grained method for simulating diffusion of a small molecule within a glassy polymer was developed and implemented. The method builds on our previous work in which molecular-level jump rates between likely sorption states were calculated with multidimensional transition-state theory incorporating explicit chain motions that accompany each jump. In this work we first use a reverse Monte Carlo approach to generate large microstructures of sorption states and jump paths whose size, connectivity, and rate constant distributions match those found in detailed molecular simulations of methane in glassy atactic polypropylene. Next we simulate diffusion of isolated penetrant molecules in these microstructures using kinetic Monte Carlo. Over small to moderate times, mean-squared displacement increases sublinearly (anomalous diffusion) in structures of either low or moderate connectivity and with either uniform rate constants or a distribution of rate constants. At long times, regular diffusion is observed in all systems except the low-connectivity structure with a distribution of rate constants. Through examination of the fraction of jumps that return to the initial state, we attribute anomalous diffusion to situations in which a penetrant molecule is confined to regions of low connectivity similar to a percolation cluster. The infrequent jumps that occur over longer times allow the penetrant to move away from this confining region and experience regular diffusion. This phenomenon is present with a distribution of connectivity and uniform rate constants, and it is exaggerated by a distribution of rate constants. The regular diffusion regime is reached for displacements beyond 70 Å and below the edge length of the periodic cell employed, and the predicted diffusion coefficient is reasonable for methane diffusing in glassy atactic polypropylene.

Introduction

Numerous products and processes, such as food packaging and membrane separations, depend on the relative permeation rates of small molecules through polymer films. For the past decade, small molecule diffusion has been investigated using molecular modeling and simulation, with the hope of identifying particular chain architectures and mechanisms that could guide the development of new polymeric materials for these applications. One difficulty, however, has been the inability of traditional molecular dynamics simulations (of duration 1−10 ns) to span the time scales relevant for diffusion in glassy polymers (microseconds and longer).

In molecular simulations (including molecular dynamics), the penetrant self-diffusivity is calculated using the Einstein relation,[1]

$$D = \lim_{t\to\infty} \frac{1}{2d} \frac{\partial \langle r_p^2 \rangle}{\partial t} \tag{1}$$

which relates the diffusivity in d dimensions to the rate of change of the average mean-squared displacement $\langle r_p^2 \rangle$ of individual penetrant species with respect to time t, at long times. Molecular dynamics (MD) simulations of penetrant diffusion[2−32] yield $r_p(t)$ by directly integrating the equations of motion, limiting their applicability to systems with diffusion constants greater than 10^{-7} $cm^2\ s^{-1}$. In systems that involve sizable energy barriers, transition-state-theory (TST)-based simulations[19,33−43] use sequences of independent penetrant jumps to determine $r_p(t)$. With both methods (applied appropriately), increases in mean-squared displacement $\langle r_p^2 \rangle$ with respect to time become linear at sufficiently long times, and a diffusion coefficient can be extracted.

Over intermediate time scales, a so-called "anomalous diffusion regime" for small-molecule penetrants in glassy and melt polymers has been observed in molecular simulations,[14,17,19,24,25,30,35,36,44] consistent with

$$\langle r^2 \rangle \propto t^n \tag{2}$$

where $n < 1$. The anomalous exponent $n = {}^1/_2$ has been seen for many systems: helium[35,36,44] and argon[36] in polycarbonate; helium,[24] methane,[17] and oxygen[24,25] in polyethylene; helium[14,36] in poly(isobutylene); and methane[17] in poly(dimethylsiloxane). An exponent $n = 0.53$ has been found in more general percolation studies.[45]

Anomalous diffusion has been observed in simulations of other systems as well. Within the zeolite silicalite, El Amrani and Kolb[46] found a short anomalous region for argon diffusion, but none was reported for diffusion of xenon[38] or aromatics.[39] Diffusion on networks described by percolating clusters have led to exponents that become increasingly anomalous as the topology progresses closer to the percolation threshold.[47,48]

† Present address: Ford Research Laboratory, Ford Motor Company, P.O. Box 2053, mail drop 3083/SRL, Dearborn, MI 48121-2053.

* To whom correspondence should be addressed.

10.1021/ma002157h CCC: $20.00
Published on Web 10/25/2001

Gusev et al.[35,36] noted that the anomalous regime seemed to end when the average root-mean-squared displacement reached the size of the simulation cell used, after which the diffusion was normal ($n = 1$). The size of the anomalous diffusion regime and its connection to elementary diffusion processes are reported here for methane in glassy atactic polypropylene, using much larger simulation cells.

Traditional methods for simulating jump-type diffusion can be subdivided into several closely linked steps: (1) generating a network appropriate for simulating jump motions (including equilibrating the surrounding chain structure and penetrant locations), (2) determining the rate constants along each path, (3) generating a sequence of jumps on that network, and (4) extracting $\langle r_p^2(t)\rangle$ over long times. The same simulation cell has typically been used for all these steps. In crystalline materials these methodologies are appropriate, since periodic replication of the unit cell correctly describes the long-range structure. However, in amorphous materials this imposes over long length scales the correlations found over short length scales in a particular configuration. Consequently, penetrant diffusion rates through amorphous polymers have potentially been calculated via simulation over a length scale equal to or longer than that of the periodic simulation cell in use and thus in the presence of periodic correlations.

We demonstrate a new approach here for generating a network appropriate for simulating diffusion that originates from jump-type motions, such as that of small molecules in glassy polymers. We then apply the method to methane diffusion through glassy atactic polypropylene. First, the small length-scale simulation cells used in our previous works[40,42,49] were reanalyzed in order to determine (1) the number of jump pathways that emanated from each void (or "sorption macrostate") in the polymer matrix and (2) the distribution of angles between consecutive jumps that a penetrant could execute. In combination with the macrostate-to-macrostate jump distance distribution (from ref 42), these properties were used in a reverse Monte Carlo simulation[50] to generate a number of large, random networks whose instantaneous site-to-site statistics agree with the macrostate distributions found in the small, atomistic structures. Each site on such a coarse-grained network corresponds to a sorption macrostate in the atomistic systems. Sorption site occupancy probabilities and jump rate constants were assigned to this network from the distributions observed in the atomistic simulations, and finally diffusion was simulated on the resulting network with kinetic Monte Carlo. This coarse graining enabled semimolecular consideration of diffusion over much longer length scales than were accessible previously, with periodic boundary conditions only arising over length scales longer than those required for normal diffusion to occur.

Simulation Methods

Network Generation with Reverse Monte Carlo. Our hypothesis regarding generation of a large network of sorption states is that if its statistically based structural and rate properties equal those calculated in atomistic polymer simulations, diffusion on this network will adequately reproduce diffusion through the atomistic polymer system. While a single large structure could technically be represented in atomistic detail on the currently largest computers, each potential energy calculation would be very slow, and identifying local minima (typically the starting point of the simulation) and equilibrating the structure would be computationally intractable. Sampling the numerous penetrant jumps that could occur would increase the intractability further.

Instead, we developed a method in the spirit of the reverse Monte Carlo method.[50−52] In reverse Monte Carlo (RMC), the objective is to find a set of particle positions whose structure factor (or radial distribution function) matches one determined experimentally.[50,53] Given any initial configuration, particle displacements are used to improve the agreement between calculated and experimental structure factors, with each move accepted or rejected with a Metropolis-type[54] criterion: if agreement improves, accept the move; if agreement worsens, accept the move with a probability proportional to $\exp(-\Delta/\chi^2)$. The term Δ represents some suitable objective function, such as the mean-squared error between the simulated and experimental structure factors. The term χ^2 plays the same role that temperature does in a typical Monte Carlo simulation: for large χ^2, fluctuations away from the target distribution increase; for small χ^2, the fluctuations become small and the target distribution corresponds to the zero of temperature. McGreevy[50] recommended using the experimental error of the measurement for χ^2; here, we used a decreasing sequence of χ^2 values to obtain good agreement (see below). For systems governed by a purely two-body potential, configurations resulting from RMC are unique in that other properties calculated from them yield essentially the same results as those calculated directly from the underlying potential.[52] For systems governed by a many-body potential, the structure factor of these configurations will match those of the underlying potential, but other properties might not agree.[55]

Here we take an analogous approach. Rather than varying atomic positions to achieve agreement with a structure factor, we vary the positions and connectivities of sorption macrostates in an off-lattice network of elementary jumps. The objective function for relaxing the network structure contains the mean-squared error relative to three probability-density distributions obtained from our molecular simulations of penetrant jump motions:[40,42,49] the number of "connections" per macrostate $p^n{}_i$, the distances between connected macrostates $p^l(l)$, and the angles between adjacent connections $p^\Omega(\Omega)$. A connection implies that some pathway exists for a penetrant to pass between the pathway's terminal positions, with concomitant polymer chain motions facilitating the jump.

To initiate the simulation, the target connectivity and jump distance distributions were renormalized to the total number of sorption macrostates N_s and the total number of jump distances $N_s N_c$, respectively, where N_c is the average number of connections per site. The instantaneous distributions of the number of macrostates with i connections ($\equiv n_i$), of the number of jump pathways with lengths between $j\delta l$ and $(j + 1)\delta l$ ($\equiv l_j$), and of the probability that a jump-to-jump angle falls between $k\delta\Omega$ and $(k + 1)\delta\Omega$ ($\equiv\Omega_k$) were tabulated; δl and $\delta\Omega$ are bin widths used to discretize the jump distance and jump angle distributions, respectively. (Note that n_i, l_j, and Ω_k are dimensionless distributions that count the number of connections, number of distances, and probability density of angles within a

structure that fall within each bin i, j, k.) The resulting objective function is

$$\Delta = \sum_i (n_i - N_s p^n{}_i)^2 + \sum_j (l_j - N_c N_s p^l{}_j)^2 + C\sum_k (\Omega_k - p^\Omega{}_k)^2 \quad (3)$$

$C \equiv N_s{}^2$ is a large constant used to scale the deviations from the jump angle distribution to place them on the same order of magnitude as deviations from the connectivity and jump-length distributions. The jump network was then varied using Monte Carlo, with the instantaneous values of the distributions (n_i, l_j, Ω_k) updated after each accepted move. Possible attempted moves consisted of displacing a site (60%), adding a new connection between two randomly selected and unconnected sites (20%) or deleting an existing connection (20%).

The initial site positions were chosen randomly within the simulation cell. Structures were generated at the sorption macrostate density found previously:[40,42] 4220 sites in a cube of edges 141.41 Å.[56] This size is about a tenth of the thickness of the ultrathin skin found on asymmetric glassy polymers used in membrane applications.[57,58] Initially no periodic boundary conditions were used, but then the average mean-squared displacement for molecules diffusing within the resulting networks reached a finite-size plateau.[59] Consequently, periodic boundary conditions were implemented in all results reported here. Approximately 10% of the desired number of bonds were made initially between unconnected pairs of sites chosen at random; the others were filled during the MC procedure. A logarithmic series of decreasing pseudo-temperatures $\chi^2 = 1000$, 100, 10, 1, and 0.1 was used to quench the sample into a local minimum.

Assignment of Realistic Sorption Probabilities and Jump Rate Constants. In order to simulate methane ghost particles in a network fully characteristic of glassy atactic polypropylene, the next step after building the jump network is to choose sorption probabilities and jump rate constants such that their distributions reflect those calculated in the atomistic simulations. Sorption coefficients were assigned first, and then jump rate constants were chosen from the distribution reported in ref 42, using a method described below.

Sorption contributes to small-molecule permeability in two respects. First, the larger the solubility S, the larger the permeability P. This contribution is separable from the diffusion contribution in the low-concentration limit ($P = DS$).[60] Second, the relative sorption within different voids is linked to the jump rate constants via microscopic reversibility,[61]

$$p_A^{eq} k_{A\to B} = p_B^{eq} k_{B\to A} \quad (4)$$

where p_A is the probability of occupying a particular macrostate A, relative to the probability of occupying any region of the polymer, and $k_{A\to B}$ is the rate to jump from anywhere in macrostate A to anywhere in macrostate B. Formally,

$$k_{A\to B} = \sum_{\substack{\text{all } i \text{ in } A \\ \text{all } j \text{ in } B}} \left(\frac{p_i}{p_A}\right) k_{i\to j} \quad (5)$$

where p_i is the probability of occupying a subset i of macrostate A in which a jump can originate and $k_{i\to j}$ is the rate of jumping from this particular state i to a particular state j in macrostate B. We have assumed that (p_i/p_A) factors can be taken equal to unity; physically, this corresponds to assuming that a penetrant is everywhere within the void at once, meaning that motions within the void are sufficiently fast for the penetrant to explore the entire void over the time scale over which a channel remains open. In our previous work,[42] almost all jumps $i \to j$ provided the only path between A and B.

The solubility within each macrostate A

$$S_A = \frac{1}{k_B T}\left\langle \exp\left(-\frac{\mathcal{V}_{pen}}{k_B T}\right)\right\rangle \quad (6)$$

was estimated using Widom ghost-particle insertions,[62,63] with void mapping[64] used to allow insertions only in those regions where geometric calculations[49] suggested a penetrant was likely to reside. The local-minimum polymer structures that formed the initial guesses for transition state searches in ref 42 were used for this purpose. Additional ghost-particle insertions using only the smallest voids were also performed in order to improve their statistics in the sorption coefficient distribution.

To assign equilibrium macrostate solubilities to the N_s sites of the jump network under consideration, the resulting probability density distribution was discretized and the normalized cumulative probabilities

$$S_n^{tot} \equiv \left(\sum_{a=1}^{n} S'_a\right)\delta S \quad (7)$$

that a sorption macrostate capacity is smaller than $n\delta S$ were calculated, where δS is a bin width and S'_a denotes the probability density for a solubility S_A to lie between $(a-1)\delta S$ and $a\delta S$. Next, for each site a random number ξ was selected between 0 and 1, and the solubility S_A for which the condition $S_{a-1}^{tot} \le \xi < S_a^{tot}$ held true was assigned to that site, subject to the constraint that sites connected to many neighbors were correlated with sites of high solubility. Finally, the relative sorption probabilities were normalized to unity. Note that no particles have yet been placed on the network; these solubilities correspond to the equilibrium concentrations toward which a set of particles would evolve.

Initial estimates for the inter-macrostate "forward" rate constants $k_{i\to j}^{TST}$ were chosen from a uniform distribution between $10^3\ \mu s^{-1}$ and $10^4\ \mu s^{-1}$, with "forward" referring to jumps from a low-probability site to a high-probability site. "Reverse" rate constants were then found from microscopic reversibility, eq 4, and the instantaneous distribution ($\equiv k_i$) of jumps with rates between $i\delta k$ and $(i+1)\delta k$ was generated. This distribution of rate constants was then evolved toward the distribution in Figure 8 of ref 42 with an RMC approach analogous to that used to generate the network structure. The only type of attempted move was to scale a rate constant pair (coupled by eq 4) by a factor between 10^{-1} and 10^1. Moves were accepted or rejected on the basis of the objective function

$$\Delta^R = \sum_{i=1}^{n} (k_i - \bar{k}_i)^2 + C' \sum_{j=n+1}^{max} j(k_j)^2 \quad (8)$$

The first term in eq 8 determines the deviation from the target distribution. The second term is a penalty function used to eliminate faster jumps. It provides a driving force for jumps with rates faster than those in the target distribution to return toward the target values. Without such a driving force, we found that some jumps would drift unbounded toward extremely fast values. Jump rates slower than those in the distribution were allowed; they block certain passages and decrease the network connectivity over time scales shorter than $1/k$. The pseudo-temperature profile used will be discussed below.

After assigning relative sorption capacities and rate constants, the network was ready for a ghost-particle simulation to begin. Analogous to the "frozen" positions of voids and channels in a glassy polymer, the relative sorption probabilities and jump rate constants remained constant throughout the diffusion simulation. After a sufficiently long simulation, ratios of ghost-particle concentrations in different sites should match the corresponding sorption probability ratios.

Simulating the Jump Process. We assume that individual penetrant jumps are uncoupled from one another and that the sequential visiting of states is a Markov process,[1] since a penetrant is likely to spend a long time exploring a sorption macrostate before jumping. Immediately after a jump, the amount of time that elapses before the next penetrant jump depends explicitly on the distribution of jump rate constants out of occupied sites. Since each jump is independent of the others, the waiting time distribution is distributed according to[1]

$$p(t)\,\mathrm{d}t = R\exp(-Rt)\,\mathrm{d}t \tag{9}$$

called a Poisson process, with R (defined below) equal to the overall jumping rate. $1/R$ is the average waiting time until the next jump will occur anywhere on the network. The sorption macrostate population then evolves according to a master equation,

$$\frac{\mathrm{d}p_A}{\mathrm{d}t} = -\sum_B\left(\sum_{j=1}^{N_B}\sum_{i=1}^{N_A}k_{i\to j}\frac{p_i}{p_A}\right)p_A + \sum_B\left(\sum_{j=1}^{N_B}\sum_{i=1}^{N_A}k_{j\to i}\frac{p_j}{p_B}\right)p_B \tag{10}$$

After some time, the macrostate probabilities stabilize at their equilibrium values p_A^{eq} that satisfy microscopic reversibility (eq 4).

Our kinetic Monte Carlo scheme to simulate the diffusion process is based on that described in ref 65. To begin, a number of independent, noninteracting "ghost" penetrants were placed on the sites of each network, according to the equilibrium distribution $p_A^{\mathrm{eq}} = S_A/\sum S_A$. The distribution was sampled after creating a cumulative distribution,

$$P_n = \sum_{i=1}^{n} S_i \tag{11}$$

using the same method as described above when assigning the sorption probabilities to each network. Ideally, the number of penetrants N_{p} should be much larger than the number of sites N_{s} in order to sample the probabilities p_A^{eq} correctly. The large networks used here necessitated using fewer ghost particles: $N_{\mathrm{p}} \approx N_{\mathrm{s}}$ or $N_{\mathrm{p}} < N_{\mathrm{s}}$. The number of penetrants in a macrostate i at a time t is denoted below by $N_i(t)$.

To begin a simulation step, the flux along each jump,

$$R_{i\to j} = N_i(t)k_{i\to j} \tag{12}$$

the total flux among all sites,

$$R = \sum_i\sum_j R_{i\to j}(t) \tag{13}$$

and their ratio, the probabilities

$$q_{i\to j}(t) = \frac{R_{i\to j}(t)}{R(t)} \tag{14}$$

were calculated. Next, the expected waiting time τ until the next event was found from

$$\tau = -\frac{1}{R}\ln(1-\xi) \tag{15}$$

with the random number ξ chosen uniformly over [0, 1). The jump executed in this next event was chosen from the probabilities $q_{i\to j}(t)$, and the particular penetrant leaving site i was chosen uniformly. Selection from $q_{i\to j}(t)$ was made in the same manner as above, using the cumulative probability density distribution. The site label for the jumping penetrant was updated, the occupancies $N_i(t)$ and $N_j(t)$ were reset to account for the jump, and the process was repeated. After a number of jump events, the average mean-squared displacement was calculated. In practice, only the fluxes out of the sites i and j that involved the most recent jump had to be recalculated according to eq 12; this decreased the number of computations significantly for a large system.

Results

Intermacrostate Properties. Three probability density distributions for the number of neighboring macrostates to which a single macrostate is connected are shown in Figure 1. The circles indicate the neighbor distribution found for intermacrostate methane jumps in glassy atactic polypropylene within our earlier transition-state theory work.[42] The triangles and squares depict the neighbor distributions found for two different hypothetical probe radii (1.9 and 1.28 Å, respectively) using computationally inexpensive geometric analysis.[49] The distributions for methane (from TST) and $r_{\mathrm{p}} = 1.9$ Å (geometry) are similar, with most sorption macrostates connected to very few (1−3) others and a small number connected to many other macrostates. The distribution for the smaller hypothetical probe indicates a higher connectivity. The solid and dashed lines in the figure are discussed below.

The angles between successive penetrant jumps were defined by all pairwise combinations of jumps that terminated in the same sorption macrostate. The distribution of angles (calculated for methane in aPP using our TST work[42]) is plotted in Figure 2. The thin dashed lines in the figure indicate the distributions suggested by combining the simulation results into different-sized bins; the distribution indicated by squares was used in the calculations below. The heavy dashed line indicates the probability density function

$$\rho(\theta) = \frac{1}{2}\sin\theta \tag{16}$$

that is appropriate for a case in which the second jump

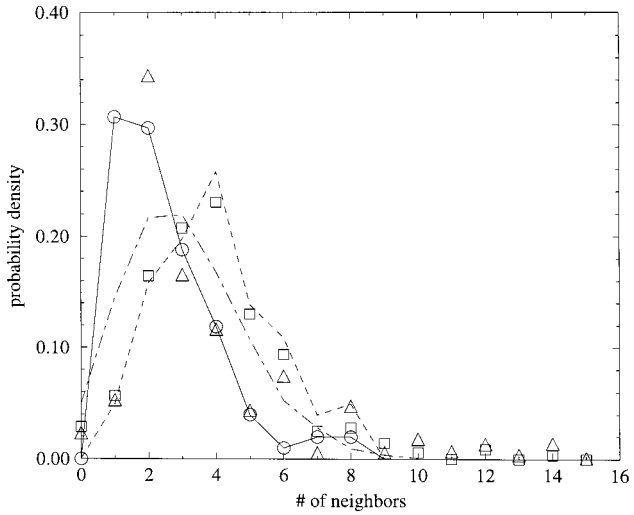

Figure 1. Neighbor distribution (connectivity among macrostates) in the TST, geometry, and RMC calculations. The circles indicate the distribution estimated for methane in aPP using TST.[42] The triangles and squares indicate the distributions estimated for hypothetical probe radii of 1.91 and 1.28 Å, respectively, using geometric analysis.[49] The solid and dashed lines indicate distributions that resulted from RMC simulations to match the methane/TST (○) and 1.28 Å/geometry (□) distributions (structures I and II). The dot−dash line indicates the connectivity in the initial guess structure used in the RMC calculations.

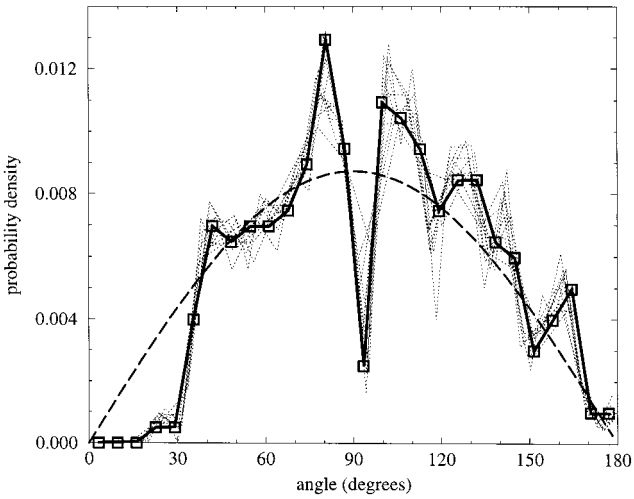

Figure 2. Jump−jump angle distributions calculated for methane in aPP, based on our earlier TST simulations.[42] Thin dotted lines indicate different distributions obtained by changing the bin size used when combining the raw data. The squares indicate the distribution chosen for use in later calculations. The thick dashed line indicates a simple random-angle model described in the text; this coincides with the initial guess distribution in the RMC calculations. The thick solid line indicates the final angle distribution found in the RMC calculations.

orientation is chosen randomly from all directions on a sphere centered at the end point of the first jump. The heavy solid line will be discussed below. The distribution from the simulations reveals concentrations of both acute and obtuse jump−jump angles. Penetrant jump pairs in which the second jump "backtracked" along the first jump path were excluded from this distribution, since they involve only one path, leading to the lack of jumps at 180°. (Sequential forward and backward jump sequences along the same path are physically realistic and were allowed in the diffusion calculations described below.) In general, the trend follows that of the random distribution, but particular regions suggest the jump orientations are not completely random. The absence of acute angles below 30° suggests that it is unlikely for distinct macrostates to lie extremely near to each other, relative to the distances along single paths from each one to a third macrostate. Fewer jumps are seen near 90° than in the random distribution. This could be a simulation artifact, because half the box size is between the average jump length and $\sqrt{2}$ times the jump length (the distance between two macrostates that form a right triangle with a third macrostate). For example, given an initial jump vector parallel to or 45° from a box-edge vector, two perpendicular jumps at the average jump length would lead to a macrostate just further from or just closer to the original macrostate than was typically found in the distribution of macrostate separations (Figure 4). Consequently, a jump at 90° could create regions between these jumps and their periodic images that are either too large or too small to fit another single macrostate. Chain relaxations would likely shift the void positions to more evenly divided separations, removing the perpendicular jump-to-jump angle. Comparing with results from others, Chassapis et al.[25] found the opposite behavior for a number of spherical oxygen united atoms diffusing simultaneously in a C_{20} melt—consecutive jumps were more likely to form angles below 40° or above 140°.

Table 1. Cooling Schedules Used To Create Network Structures I and II with Reverse Monte Carlo

run no.	no. of moves: in run	no. of moves: cumul	pseudo-T	fraction moves successful: posn	fraction moves successful: add bonds	fraction moves successful: del bonds
			(a) Structure I			
1	2.5×10^7	2.5×10^7	1000	0.793	5.58×10^{-2}	5.66×10^{-2}
2	2.5×10^7	5.0×10^7	100	0.387	1.30×10^{-2}	1.25×10^{-2}
3	2.5×10^7	7.5×10^7	10	0.087	2.08×10^{-3}	1.97×10^{-3}
4	2.5×10^7	10.0×10^7	1	0.421	2.44×10^{-3}	2.45×10^{-3}
5	5.0×10^7	15.0×10^7	0.1	0.268	3.70×10^{-6}	2.90×10^{-6}
			(b) Structure II			
1	2.5×10^7	2.5×10^7	1000	0.715	4.47×10^{-2}	4.59×10^{-2}
2	2.5×10^7	5.0×10^7	100	0.087	3.15×10^{-3}	2.38×10^{-3}
3	2.5×10^7	7.5×10^7	10	0.024	6.99×10^{-4}	5.80×10^{-4}
4	2.5×10^7	10.0×10^7	1	0.273	1.70×10^{-3}	1.70×10^{-3}
5	5.0×10^7	15.0×10^7	0.1	0.171	5.00×10^{-5}	4.96×10^{-5}

The neighbor distribution (connectivity), the jump distance distribution,[66] and the jump angle distribution characterize the two-state and three-state structural correlations for sorption macrostates in atactic polypropylene, as probed by molecular simulations on the 25 Å length scale. We next used that information with the methods described in the previous section to generate much larger representative structures of sorption macrostates.

Jump Network (Structure) RMC. Two large cubic structures (edge length = 141.4 Å) were created using the RMC procedure. Structure I was based on the lower connectivity found for methane in the TST calculations as a "target"; structure II was based on the higher connectivity found for r_p = 1.28 Å in the geometric analysis (see Figure 1). The sequence of decreasing pseudo-temperatures used to relax the network structures and the fractions of accepted moves are listed in Table 1. The decrease in the structure-generation objective function Δ vs increasing cumulative total number of attempted moves is shown in Figure 3 for structures I and II. At the higher pseudo-temperatures, Δ decreased significantly before reaching a level about which it fluctuated for a number of moves. Significant fractions

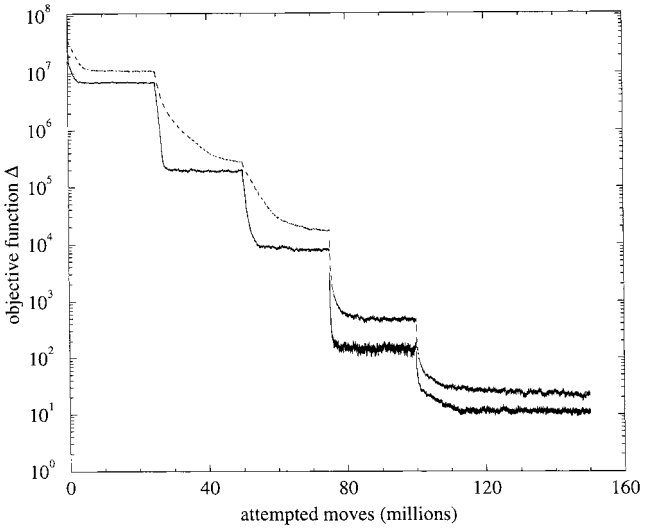

Figure 3. Changes in the objective function during network structure generation for structures I and II (lower and upper lines, respectively). Changes in slope indicate points where the pseudo-temperature was changed.

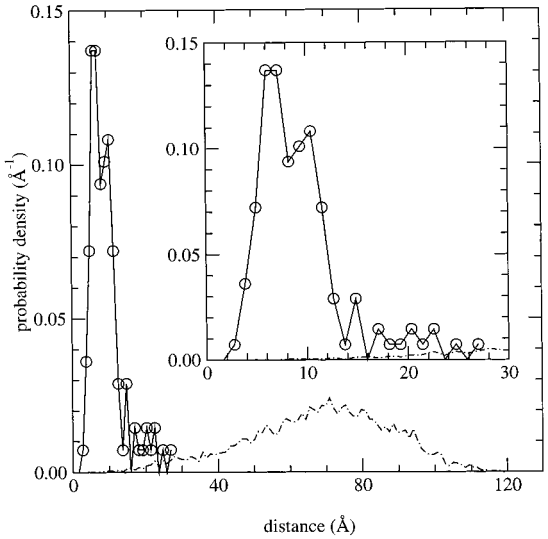

Figure 4. Target, initial, and final distribution of the distances between connected neighbors. The target distribution comes from Figure 11 of ref 42 and is indicated by circles. The lines represent the initial (dot−dash line) and final (solid line) distributions generated by RMC for structure I; lines for structure II overlap those shown. The inset highlights the small-distance region, in which the only remaining jump distances were located.

of position moves were accepted at all pseudo-temperatures, while the fraction of accepted connection additions/deletions decreased significantly with decreasing pseudo-temperature.

The initial and final neighbor, jump angle, and distance probability density distributions for structure I are compared to the target distributions in Figures 1, 2, and 4. Solid lines indicate the final distributions. In Figures 1 and 4, dot−dash lines indicate the initial distributions; in Figure 2 the initial distribution falls on the heavy dashed curve that represents random orientations. The final neighbor distribution for structure II is indicated in Figure 1 by a dashed line; the jump angle and distance final distributions coincide with those found for structure I. The final distributions were calculated in each case from the single structure at the completion of the network generation. It was not

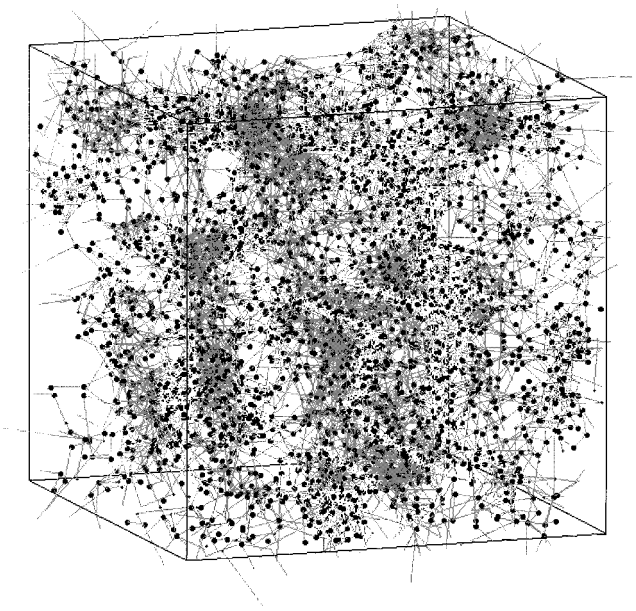

Figure 5. Visualization of the moderate-connectivity network created by RMC. The box edge is 141.4 Å. See text for details.

necessary to average over a number of different structures, since the system was large enough to be "self-averaging": enough different environments (states of connectivity) existed within each structure to represent the ensemble adequately. The agreement between the target and final distributions illustrates the power of RMC: a collection of sites showing the desired structural correlations can be generated successfully. Agreement is "too good", in that deviations from the target distributions in the final structure are smaller than the underlying errors in the target distributions.

The final configuration of macrostates and macrostate connectivity in structure II (moderate connectivity) is illustrated in Figure 5. The macrostate centers are indicated by dark spheres; larger spheres indicate higher solubility. The connections among macrostates are indicated by gray lines. The connections that appear to exit the simulation cell are connected to periodic images of macrostates. Apart from the randomly assigned solubility, no particular volume or shape was attributed to each macrostate. However, the connectivity distribution led to a spatial distribution of macrostate density. A macrostate with many neighbors is, by definition, surrounded by many other macrostates; these macrostates each have neighbors of their own, causing the local enhancement in density. The result is a fluctuation in macrostate density over length scales larger than the size of the molecular simulation cells used to generate the target distributions. (Typically 6−7 simulation cells would span each edge of the box pictured in Figure 5.) The large connectivities, which are most responsible for the larger fluctuations in macrostate density, were found with the poorest statistics in the molecular simulations.[49] Consequently, these larger fluctuations are more prone to sampling errors from the smaller-scale simulation.

Diffusion on Network with Uniform Sorption Coefficients and Jump Rate Constants. The jump network created by the RMC procedure is fairly disordered compared to a crystalline array of sites, such as a three-dimensional cubic lattice. The closest crystal-like relative would be a percolation cluster created by removing some of the site−site links between adjacent

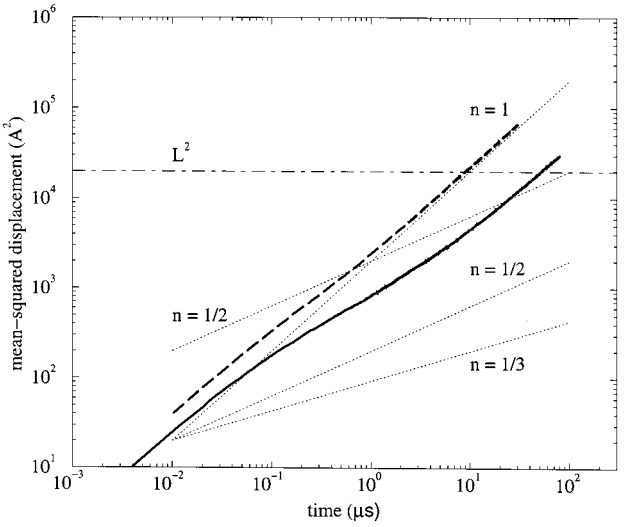

Figure 6. Mean-squared displacement as a function of time for ghost particles on structures with equal sorption probabilities and rate constants equal to 10 μs^{-1}. Diffusion on the structures with higher and lower connectivities is indicated by the upper thick dashed and lower solid lines, respectively. The dotted lines have slopes of 1, $^1/_2$, and $^1/_3$; see text for details. The dot−dashed line indicates the box size squared.

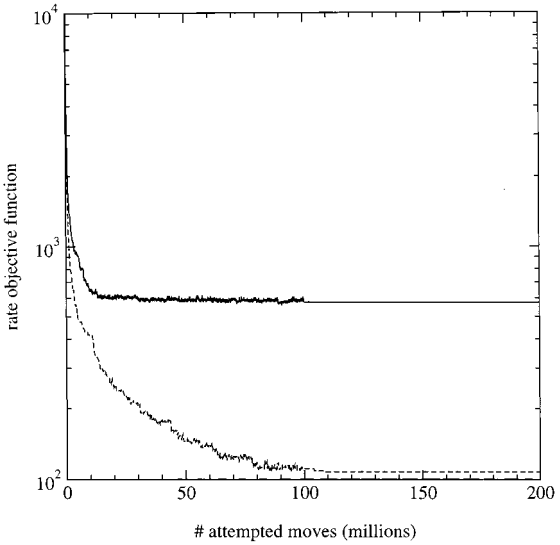

Figure 7. Convergence of jump rate constants toward the target distribution (Figure 8 of ref 42). Each attempted move either increased or decreased a single rate constant pair assigned to the network. The objective function Δ^R is defined in the text. Upper and lower curves correspond to low and moderate connectivities, respectively.

sites.[67] Since unusual effects have been noted for diffusion on percolation clusters (such as de Gennes' "ant in a labyrinth" problem[68]), diffusion on the generated jump network was first investigated without applying a distribution of sorption coefficients and jump rate constants. Instead, all sorption coefficients and site−site jump rate constants were set equal to one (in dimensionless units) and 10 μs^{-1}, respectively.

Two kinetic Monte Carlo simulation runs were conducted on structures I and II. First, 5000 ghost particles were assigned randomly to the 4220 sites. The initial site positions were stored, and the continuous-time discrete-space kinetic Monte Carlo procedure was used to track the time evolution of ghost-particle site occupancies. The number of jumps that resulted in a ghost penetrant returning to its initial site was also recorded.

The average mean-squared displacements in these structures are shown in Figure 6 as a function of time. The fractions of jumps denoting returns relative to the initial structure are shown in Figure 10 as a function of mean-squared displacement and will be discussed below. Averaging was performed over all the ghost particles but without averaging over different time origins. The thin dotted lines denote the curves for scaling exponents $n = 1$, $^1/_2$, and $^1/_3$. Within structure I, three regimes are noticeable for the mean-squared displacement (solid curve). Initially, its increase with time is nearly parallel to the $n = 1$ line. At about 0.1 μs, the increase in average mean-squared displacement slows down and begins to follow a rate proportional to $t^{1/2}$. At longer times near $t = 6-7$ μs, the increase in mean-squared displacement speeds up and is again nearly proportional to time. Within structure II, changes in slope occur at similar times but are much smaller; the increase in mean-squared displacement is linear after approximately $t = 1$ μs. Since the average mean-squared displacement is larger, diffusion occurs faster in structure II.

Diffusion on a Network with Realistic Probabilities and Rate Constants. Next, we assigned sorption coefficients and macrostate-to-macrostate jump rate constants characteristic of methane in glassy atactic polypropylene to structures I and II. The pseudo-temperature profile in Table 2 was followed to equilibrate the site−site jump rate constants. Evolution of the objective function (eq 8) is shown in Figure 7 for both structures. Final agreement with the target distribution was reasonable in both cases. The system with realistic probabilities and rate constants was then simulated in a manner analogous to that for the system with uniform rate constants and sorption probabilities. For each structure, 2000 ghost particles were placed on the 4220 sites according to the sorption coefficient distribution. Continuous-time discrete-space kinetic Monte Carlo was then used to track the evolution of the ghost-particle population.

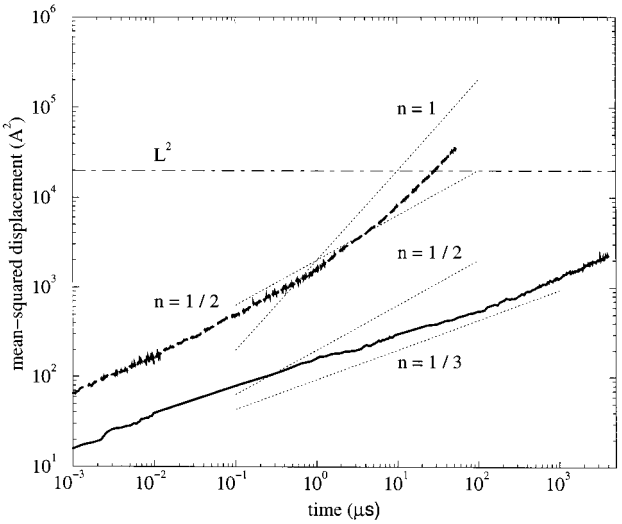

Figure 8. Mean-squared displacement as a function of time for ghost particles on a network with realistic rate constants and sorption probabilities. Labels are the same as in Figure 6.

The average mean-squared displacements are shown as functions of time in Figures 8 and 9 (logarithmic and linear coordinates, respectively). The fractions of jumps

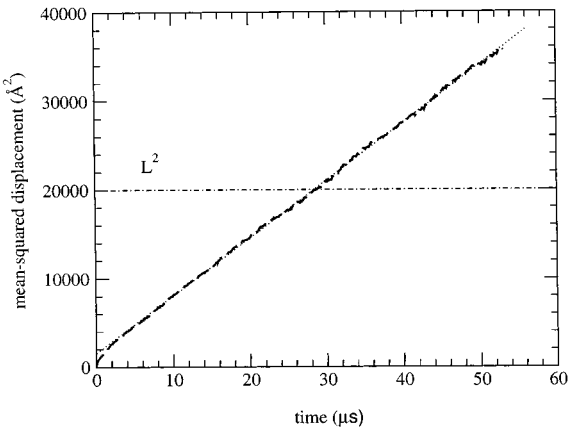

Figure 9. Similar curve to Figure 8, but in linear coordinates. The curve for the structure with low connectivity is not shown since the linear regime was not reached. The dotted line indicates a linear slope corresponding to $D = 1.08 \times 10^{-8}$ cm^2 s^{-1}.

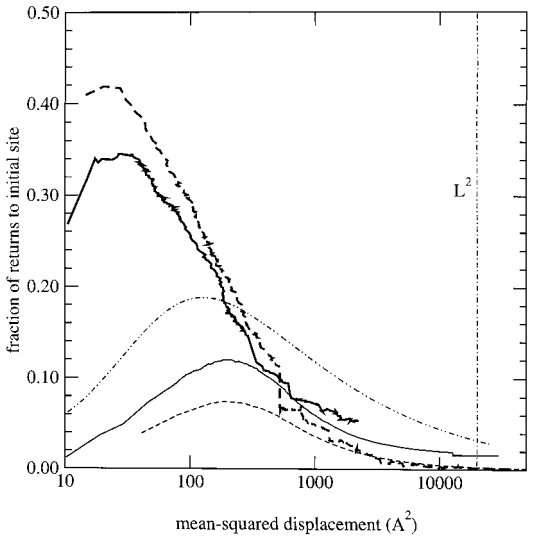

Figure 10. Fraction of jumps in which penetrants returned to their initial starting positions as a function of mean-squared displacement. The thin solid and dashed lines indicate results for the low and moderate connectivity structures, using equal sorption probabilities and rate constants. The heavy solid and dashed lines indicate results for the same structures using realistic sorption probabilities and rate constants. The vertical dot−dash line indicates the box size squared. The other dot−dash line indicates analytical results from a one-dimensional random walk model.

Table 2. Different Rate Assignments to the Network Structures Created with Reverse Monte Carlo[a]

		no. of moves		rate objective function	
run no.	pseudo-T	in run	cumul	Δ (I)	Δ (II)
init.				4.8×10^6	2.5×10^7
1	0.4	1×10^8	1×10^8	593.1	112.4
2	0.08	1×10^8	2×10^8	573.9	107.6

[a] The objective functions for the two structures are indicated in the two rightmost columns. Each run leads to a different jump network on which diffusivity calculations may be carried out.

that caused returns to the initial site are shown as a function of mean-squared displacement in Figure 10. The thin dotted lines in Figure 8 indicate scaling exponents $n = 1$, $n = 1/2$, and $n = 1/3$. Within structure I, after some initial noise the diffusion exponent appears smaller than $n = 1/3$ at small times. It then increases to between $1/3$ and $1/2$ at an average mean-squared displacement of 500−600 Å^2, slightly higher than the onset point for anomalous diffusion in the network with uniform rate constants. It was not possible to reach the linear diffusive regime ($n = 1$) in this structure, as seen in Figure 8. Within structure II, the diffusion exponent equals $n \approx 1/2$ for small times and increases to unity at longer times (greater than 5 μs). This turnover occurs at an average mean-squared displacement of 5000 Å^2, which is similar to where a linear increase was found to set in in the simulations with uniform rate constants. The linear region within structure II is also clearly seen in Figure 9 by the heavy dashed curve. The thin dotted line in Figure 9 indicates the Einstein relation (eq 1) with $D = 1.08 \times 10^{-8}$ cm^2 s^{-1}. After the linear regime is reached at $t \approx 5$ μs, the diffusion rate is constant. The dot−dash line indicates a mean-squared displacement equal to the box size squared. The linear diffusion regime has been reached long before the average ghost penetrant revisits images of its original sites.

The cumulative fractions of jumps that resulted in ghost penetrants returning to their initial site are shown in Figure 10 as a function of mean-squared displacement for all four sets of diffusion calculations. Thin lines indicate results from the simulations with equal sorption probabilities and rate constants. Thick lines indicate results from the simulations with realistic sorption probabilities and rate constants. Results from simulations with the low or moderate connectivity structures are distinguished by solid and dashed lines, respectively. The dot−dashed line indicates the results from a model described next.

A model for this process may be constructed by considering a one-dimensional random walk. Jumps between sites are governed by the master equation

$$\frac{dp_i}{dt} = k'p_{i-1} + k'p_{i+1} - 2k'p_i \tag{17}$$

and all jump rate constants k' are assigned the same value $k' = 10$ μs^{-1}. For an initial site occupancy probability distribution $p_i(0) = \delta_{i0}$ (Kronecker delta), the time evolution can be solved analytically, yielding[1]

$$p_{\pm 1} = (\exp -2k't)[k't + (k't)^3/2 + (k't)^5/12 + (k't)^7/144 + ...] \tag{18}$$

A "return" in this model is defined as a jump from either of sites $i = \pm 1$ back to site $i = 0$. The rate of such jumps occurring equals $(p_{-1} + p_1)k'$ from eq 17. The total jump rate equals the sum over all jump rates out of each site,

$$\sum_i \left(\frac{dp_i}{dt}\right)_{\text{out}} = \sum_i 2k'p_i = 2k' \tag{19}$$

and thus the fraction of jumps at time t that are returns to the original site $i = 0$ equals $(p_{-1}(t) + p_1(t))/2$. The cumulative fraction of jumps equals the time average,

$$f(t) = \frac{1}{t}\int_0^t \frac{p_{-1} + p_1}{2}\, dt \tag{20}$$

Mean-squared displacement is calculated directly from $\langle r^2 \rangle = 2k'l^2t$, with $l = 6.04$ Å chosen so the diffusion coefficient in this simple model matches that for the moderate connectivity structure with equal rate con-

stants. The cumulative fraction is plotted vs mean-squared displacement $\langle r^2 \rangle$ in Figure 10.

For the simple model, the cumulative fraction of returns rises smoothly until a mean-squared displacement of ~100 Å^2 and then falls. From eqs 18 and 20, this pattern corresponds to the rise and subsequent fall in the probability that a ghost penetrant will occupy a site adjacent to the original site.

For the simulations with equal sorption probabilities and rate constants, there are initially very few returns to initial sites. Most jumps are by penetrants leaving their initial state. Since each site has more neighbors than in the simple model, the probability of occupying any particular site is smaller, and hence, in analogy to eq 20, the fraction of returns is smaller. With increasing time, the fraction of returns reaches a peak value that depends on the average connectivity (the larger the connectivity, the more spread in the probability distribution and the smaller the peak value of the fraction of returns) and then decreases as penetrants diffuse away from their initial locations.

The fractions of returns are initially much larger for the simulations with realistic sorption probabilities and rate constants. Particular penetrants are more likely to jump (due to the distributions), and their shuttling motions among neighboring states increase the fraction of returns compared to that found in the uniform distribution cases. Following eq 20, those particular sites have much higher occupancy probabilities at small mean-squared displacements. After significant mean-squared displacements have occurred (i.e., long times), the fractions of returns for the realistic cases fall to those of the uniform distribution cases. This underlying similarity indicates that the fraction of returns relates to the underlying geometry of the penetrant diffusion network, over times long enough for significant diffusion to occur. Significantly, this convergence occurs before the mean-squared displacement equals the box size squared. The small fractions that remain indicate that a few penetrants remain trapped in their initial state even after the mean-squared displacement becomes substantial.

Discussion

Several researchers have found anomalous diffusion in simulations of penetrant diffusion through glassy polymers. Müller-Plathe et al.[14] and Gusev et al.[19] attributed the anomalous diffusion regime to two factors: (1) the restriction by the polymer of the allowed penetrant paths, which consequently cannot be random; (2) the separation of time scales between in-cavity and long-range motions. Müller-Plathe also raised an analogy with diffusion on percolating clusters,[47,48] in which many examples of anomalous diffusion can be found. The percolation cluster analogy is very appropriate for the present work and consequently will be discussed in detail. Weber and Paul[45] found that the crossover mean-squared displacement to normal diffusion increased with system size until a plateau value was reached. Cuthbert et al.[30] found that the anomalous exponent and the crossover mean-squared displacement depended on the penetrant size.

In diffusion simulations on random networks, diffusion rate anomalies appear at connectivities near the percolation threshold and describe how the diffusivity exponent changes from $n = 0$ (a small, finite region) to $n = 1$ (an infinitely large region),[67] depending on how the time of interest compares to the deviation from the percolation threshold—the anomalous region increases in duration as the system approaches the threshold.[67] Stauffer and Aharony predict exponents of $n = 0.66$ in two dimensions and $n = 0.4$ in three dimensions at the percolation threshold.[67] A wide variety of exponents (depending on the specific lattice type and rate constant distribution) were summarized in reviews.[47,48] This work differs from those summarized in that most disordered materials have been studied by applying a distribution of rate constants to an ordered lattice, rather than applying uniform or distributed rate constants to a disordered lattice.

Some simulations of lattice gases have been conducted on ordered networks, with sufficient numbers of sites or bonds removed in order to reach the percolation threshold. (In three dimensions a fraction $p_c = 0.3116$ of the sites remain occupied.) Roman[69] studied a three-dimensional system with noninteracting ghost particles; he calculated an exponent of $n = 0.38 \pm 0.02$ for the mean-squared displacement. Paetzold[70] studied a similar system, but with multiple occupancies of sites forbidden. For a concentration of 10% (relative to the number of sites on the percolating cluster), he found that an exponent $n = 0.366 \pm 0.020$ governed the mean-squared displacement with respect to time. These results clarify what exponents could be observed in penetrant/polymer systems if the networks of traversed pathways resemble percolating clusters.

One question that still remains is that the penetrant jump networks here are disordered, and they do not necessarily resemble a regular lattice with some sites or bonds removed. Studies of the direct-current conductivity exponent, which is exactly analogous to the diffusion exponent,[67] have shed some light on this situation. Halperin et al.[71,72] addressed the continuum-vs-discrete issue to some extent in the context of the Swiss cheese model (the properties of the solid that remains after spherical holes have been removed).[73−75] They found that the conductivity exponent increased relative to its value in a discrete network. They also emphasized that the particular distribution of transport rates could affect the conductivity exponents.

Significant early studies of conductivity were conducted by Pike and Seager.[76,77] They established by Monte Carlo simulation the percolation thresholds and critical numbers of bonds per site for a number of regular lattices in two and three dimensions. They also found that conduction was well-described by a percolation-type approach near p_c: conductivity (and diffusivity by analogy) is limited by the resistance (or barrier height) of a few key pathways. Further from the threshold, an effective-medium approach[78] is appropriate, so long as the distribution of resistances is not too broad.[79] Such an approach has recently been applied by Karayiannis et al.[80]

With the context for anomalous diffusion established, we next discuss the kinetic Monte Carlo simulation findings of this work. The observed increases in mean-squared displacement with respect to time can be classified (as in ref 19) into three regimes: linear at small times, sublinear at intermediate times, and linear again at longer times. In the first regime, all early jumps constitute escapes from one (or a few) initial sites under a first-order process; this leads to linear increases in average mean-squared displacement with respect to time.[59] The fraction of jumps that return ghost particles

to their initial site increases during this regime, signifying the ever-increasing population that reside one jump away from their initial site.

The second regime can be explained as a two-part process. First, the fraction of jumps that bring ghost particles back to their initial states has continued to increase; this signifies even larger populations in sites one jump removed from their initial sites. This fraction then decreases, indicating that ghost particles are spreading further away. In a continuum, this would signify the onset of diffusive behavior: $\langle r^2 \rangle \propto t$. However, only a few pathways are available out of each site, and each leads to another site from which few pathways are available. Over the length scale of the few most probable jump pathways, the path traced *by the pathways themselves* resembles a random walk, so

$$|\mathbf{R}(\text{after } m \text{ jumps}) - \mathbf{R}(\text{initial})|^2 \propto m \qquad (21)$$

where m is the number of jumps. However, the ghost particles are now limited to following this random-walk-like pathway. On average, after a time t a particle will only displace itself by $m \propto t^{1/2}$ jumps and thus

$$\langle r^2 \rangle \propto t^{1/2} \qquad (22)$$

The second regime is subdiffusive (or "anomalous") since diffusive motions are limited to a pathway defined on a random walk (a random walk on a random walk[81]). In the runs with equal rate constants, the mean-squared displacement increases sufficiently faster than would be found at the percolation threshold to state that the connectivity available on this time scale is above the threshold. In the context of the explanations of anomalous diffusion by Müller-Plathe et al. and Gusev et al., this suggests that the anomalous regime is related to the first explanation: penetrant motion is restricted at short time scales to few allowed paths.

The third regime represents true diffusion. The paths followed by ghost particles have extended far enough so that they detect the connectivity and dimensionality of the network. The average mean-squared displacement by ghost particles has now exceeded the size of obstacles presented by nonexistent linkages or indirect connections. The diffusivity in this regime, evaluated from the Einstein relation (eq 1), equals 6.1×10^{-9} and 36.5×10^{-9} cm^2 s^{-1} for the low- and moderate-connectivity systems with equal rate constants. A simple estimate for the diffusivity $D = (z/6)kl^2$ can easily be checked at this stage. From Table 1 of ref 42, an average jump length $l = 10.3$ Å or $l = 7.40$ Å can be considered typical, depending on whether an arithmetic or geometric mean is chosen. The rate constant equals $k = 10\ \mu s^{-1}$ for all jumps in these uniform-rate runs. The average connectivity is 2.5 and 4.0 for structures I and II, respectively. For the low connectivity, the simple model predicts $D = 44.3 \times 10^{-9}$ cm^2 s^{-1} or $D = 22.8 \times 10^{-9}$ cm^2 s^{-1} for the arithmetic or geometric mean jump length, respectively. For the moderate connectivity, the simple model predicts $D = 71.0 \times 10^{-9}$ cm^2 s^{-1} or $D = 36.5 \times 10^{-9}$ cm^2 s^{-1}, respectively. The diffusivity calculated from simulation for the low connectivity is slightly smaller than that estimated by the simple model, while the diffusivity found for the moderate connectivity is comparable from both approaches. These results suggest that this simple model is capable of predicting the diffusion coefficient when all rate constants are equal.

The simple model does not fare as well in the presence of a rate constant distribution. For moderate connectivity, a diffusivity of $D = 10.8 \times 10^{-9}$ cm^2 s^{-1} was calculated from the simulation with a rate constant distribution present. Applying the simple model with the arithmetic mean jump length leads to an effective mean rate constant of $3.0\ \mu s^{-1}$. Multiplying the uniform rate constant of $10\ \mu s^{-1}$ by the ratio of the diffusivities in the presence or absence of the distribution also yields an average rate of $3.0\ \mu s^{-1}$. Comparing to the rate constant distribution used in creating the system (Figure 8 of ref 42), approximately 56% of jumps have this rate or faster. This corresponds to an average of 2.3 bonds per jump site, which is slightly smaller than the 2.7 required to reach the percolation threshold in a system of random nearest-neighbor bonds.[76] Pike and Seager[76] suggested that this particular jump rate (corresponding to the time at which the bond network first percolates) is the proper rate constant to use in this type of simple model. For our system, such an approach leads to a reasonable but not quantitative estimate of the diffusion coefficient. To exceed a connectivity of 2.7 jumps per sorption site in the moderate-connectivity system, jumps with rates in the range $0.1-1.0\ \mu s^{-1}$ must be included, which would suggest an effective jump rate a factor of 10 smaller than that calculated with the simple model.

The diffusion coefficient we have predicted from molecular simulation for methane through glassy atactic polypropylene cannot be compared directly with experimental data. (We are not aware of any such data in the literature.) Instead, we provide two alternative comparisons. First, diffusion coefficients and activation energies have been reported[82] for argon and nitrogen in an ethylene/propylene copolymer that has 31 methyl groups per 100 carbon atoms. Extrapolating those diffusion coefficients using the relation

$$D = D_0 \exp\left(-\frac{E_D}{RT}\right) \qquad (23)$$

leads to diffusion coefficients of 16.7×10^{-9} and 5.6×10^{-9} cm^2 s^{-1} for argon and nitrogen, respectively, at 233 K. Second, the diffusion coefficient can be estimated using correlations from van Krevelen.[83] As input, these correlations require the penetrant size ($\sigma = 3.76$ Å)[83] and the polymer glass temperature (255 K). The resulting estimate is 1.0×10^{-10} cm^2 s^{-1} for the diffusion coefficient.

The appropriate diffusion coefficient from this work to compare against these extrapolations and correlations is the value 10.8×10^{-9} cm^2 s^{-1} found for the moderate connectivity network with a distribution of rate constants. Agreement is excellent with the extrapolated values for the ethylene/propylene copolymer. Within that copolymer, we expect the methane diffusion coefficient would fall between the argon and nitrogen values because it has an intermediate size. The diffusion coefficient we predict falls within that same range. Agreement is not as good with the diffusivity estimated by correlation; we predict that methane would diffuse 2 orders of magnitude more quickly than is predicted by correlation. Presumably both methods are subject to error during the extrapolation to low temperature, and it is reasonable to expect that the true diffusion coefficient for methane in atactic polypropylene falls in between these extrapolated values.

For the moderate- and low-connectivity uniform rate systems and the moderate-connectivity system with a distribution of rate constants, the crossover from the anomalous to the diffusive regime occurs near $\langle r^2 \rangle^{1/2} \approx$ 41, 55, and 67 Å, respectively. All these distances are larger than the edge lengths used in the molecular simulations referenced in the Introduction. This suggests that the onset of diffusion at lower root-mean-squared displacements in those cases is an artifact of the system size. While the particular crossover mean-squared displacement would depend on the polymer of interest (and has been suggested to depend on the penetrant[30]), the TST picture of diffusion predicts the crossover would be similar for similar penetrants in the same polymer, since similar three-dimensional diffusion paths would be followed. It also suggests that the disappearance of anomalous diffusion in previous simulations at root-mean-squared displacements comparable to the box length is a simulation artifact. A diffusing penetrant, after traveling a box length L over an average time τ in a system with periodic boundary conditions, finds itself in a position essentially identical to its starting point. Diffusing the next L units will also require a time τ (on average); hence, the mean-squared displacement will increase linearly over times significantly larger than τ, the time required to take a step of size L from a coarse-grained perspective. This work differs in that the normal diffusion regime is reached well before the mean-squared displacement equals the box-size squared. On the basis of the transition from anomalous to regular diffusion, we estimate that a length scale of 67 Å corresponds to the size of correlated pathways for methane and similar-sized penetrants in polypropylene. This length is of the same order as the size of macrostate density fluctuations; hence, the exact value could be affected by sampling errors in deriving the original connectivity distribution. However, since even the better sampled connectivities are above those required (on average) to exceed the percolation threshold, we expect this picture is qualitatively correct.

The many exponents arising from percolation theories of diffusion aid in interpreting the various regimes observed here. The anomalous exponent $n = {}^1/_2$ is larger than those for diffusion on percolation clusters but matches the exponent for random-walk diffusion along a random walk, suggesting that the latter is more descriptive of the paths followed by diffusing penetrants over intermediate to long time scales. At shorter times in the network with rate constants and sorption probabilities reflective of methane in atactic polypropylene, the exponent is smaller than those found for diffusion on a percolating cluster. A logical inference is that the geometry over this time scale more closely resembles that of a percolating cluster. An occasional site acts like a "cul-de-sac", and the time spent exploring it is wasted in terms of net penetrant displacement. After longer times, the probability of these slow channels having opened at some point is larger, and thus the geometry of the structure more closely resembles an infinite cluster at $p > p_c$ rather than a percolating cluster at $p \approx p_c$. The diversity in rate constants expands the range of subdiffusive behavior (the extended size of the anomalous regime in Figure 8 as compared to that in Figure 6), but the distribution of geometric connectivity on the network (in particular the presence of sites with low connectivity) is sufficient to cause anomalous diffusion. The increase and decrease in the fraction of jumps that are returns to an initial site support the argument that anomalous diffusion in these separate cases is due to the same underlying geometric cause but over different times.

An implication of this result is that the concept of a "macrostate" of local penetrant-location (free energy) minima is not simply limited to one separation of length or time scales. Visualization of the jump network (Figure 5, see also ref 59) reveals dense sorption site patches near sites that exhibit high connectivities. The probability of overcoming a barrier (such as a particular slow jump path) within such a region is much larger than the probability of overcoming the same barrier between collections of macrostates; in the former case there are likely many circuitous routes that are greater in distance but faster in elapsed time. Over a micron length scale, there appear to be macrostates of macrostates, and net diffusion would be limited by the rate at which penetrants could travel between these "macromacrostates". It is not clear whether such hierarchies would continue to emerge as the length scales of interest increased, but it is certainly possible.

Conclusions

In this paper, we have developed methods for estimating penetrant diffusivity that are less susceptible to the small length-scale problems inherent in typical molecular simulations. In particular, we showed how an extremely large disordered network of sites could be generated for simulating penetrant diffusion. The short length-scale properties of this network were matched to the results of the atomistic level simulations. Site occupancy probabilities and jump rate constants between sites were governed by the statistics determined with our previous transition-state theory simulations.[40,42] Their combination has resulted in a coarse-graining method capable of predicting penetrant diffusion over long length scales.

A reverse Monte Carlo simulation was capable of replicating the site density, jump length, and jump-to-jump angle distributions that were observed in the atomistic simulations within a much larger system. RMC was then used to match the sorption coefficient and jump rate constant distributions found in the atomic systems, with correlations incorporated between large sorption coefficients and large numbers of connections. The diffusion behavior extracted from kinetic Monte Carlo simulations for networks with equal rate constants and sorption probabilities and low or moderate connectivities reproduced the behaviors present in prior simulations, indicating that the anomalous regime over moderate time scales is due (at least in part) to the randomness of the underlying jump network. Runs on a network with sorption probabilities and jump rate constants reflective of methane in glassy atactic polypropylene with moderate connectivity displayed a longer anomalous region, which resembled the anomalous region noted in prior simulations and in the equal rate constant run here, followed by a linear regime. For the system with realistic sorption probabilities and rate constants but low connectivity, a smaller exponent was observed and no linear regime was reached; the breadth of the rate constant distribution prevented these simulations from reaching the diffusive regime within a reasonable computation time. The fraction of jumps that returned a penetrant to its initial state (as a function of mean-squared displacement) indicated that the mech-

anism of anomalous diffusion in these separate cases was due to the same underlying geometric cause. The qualitative shape of this fraction agreed with analytical predictions based on a one-dimensional random walk model. Differences in the rate constant distribution led to anomalous diffusion occurring over different time scales but by the same mechanism. The diffusivity extracted from the moderate-connectivity network with a rate constant distribution taken from the results of atomistic TST analysis is ca. 10^{-8} cm^2 s^{-1}. This value for methane in glassy atactic polypropylene is faster than predicted using correlations developed near room temperature. However, the predicted diffusivity is in reasonable agreement with extrapolations from room-temperature measurements on argon and nitrogen diffusion in an ethylene/propylene copolymer.

References and Notes

(1) van Kampen, N. G. *Stochastic Processes in Physics and Chemistry*, revised edition; North-Holland: Amsterdam, 1992.
(2) Trohalaki, S.; Rigby, D.; Kloczkowski, A.; Mark, J. E.; Roe, R. J. *Polym. Prepr.* (*Am. Chem. Soc., Div. Polym. Chem.*) **1989**, *30* (*2*), 23−24.
(3) Takeuchi, H. *J. Chem. Phys.* **1990**, *93*, 2062−2067.
(4) Sonnenburg, J.; Gao, J.; Weiner, J. H. *Macromolecules* **1990**, *23*, 4653−4657.
(5) Takeuchi, H.; Roe, R.-J.; Mark, J. E. *J. Chem. Phys.* **1990**, *93*, 9042−9048.
(6) Takeuchi, H.; Okazaki, K. *J. Chem. Phys.* **1990**, *92*, 5643−5652.
(7) Takeuchi, H. *J. Chem. Phys.* **1990**, *93*, 4490−4491.
(8) Müller-Plathe, F. *J. Chem. Phys.* **1991**, *94*, 3192−3199.
(9) Boyd, R. H.; Pant, P. V. K. *Macromolecules* **1991**, *24*, 6325−6331.
(10) Takeuchi, H.; Okazaki, K. *Makromol. Chem., Macromol. Symp.* **1993**, *65*, 81−88.
(11) Sok, R. M.; Berendsen, H. J. C.; van Gunsteren, W. F. *J. Chem. Phys.* **1992**, *96*, 4699−4704.
(12) Müller-Plathe, F. *J. Chem. Phys.* **1992**, *96*, 3200−3205.
(13) Müller-Plathe, F.; Rogers, S. C.; van Gunsteren, W. F. *Macromolecules* **1992**, *25*, 6722−6724.
(14) Müller-Plathe, F.; Rogers, S. C.; van Gunsteren, W. F. *Chem. Phys. Lett.* **1992**, *199*, 237−243.
(15) Smit, E.; Mulder, M. H. V.; Smolders, C. A.; Karrenbeld, H.; van Eerden, J.; Feil, D. *J. Membr. Sci.* **1992**, *73*, 247−257.
(16) Pant, P. V. K.; Boyd, R. H. *Macromolecules* **1993**, *26*, 679−686.
(17) Tamai, Y.; Tanaka, H.; Nakanishi, K. *Macromolecules* **1994**, *27*, 4498−4508.
(18) Han, J.; Boyd, R. H. *Macromolecules* **1994**, *27*, 5365−5370.
(19) Gusev, A. A.; Müller-Plathe, F.; van Gunsteren, W. F.; Suter, U. W. *Adv. Polym. Sci.* **1994**, *116*, 207−247.
(20) Zhang, R.; Mattice, W. L. *J. Membr. Sci.* **1995**, *108*, 15−23.
(21) Gee, R. H.; Boyd, R. H. *Polymer* **1995**, *36*, 1435−1440.
(22) Han, J.; Boyd, R. H. *Polymer* **1996**, *37*, 1797−1804.
(23) Hofmann, D.; Ulbrich, J.; Fritz, L.; Paul, D. *Polymer* **1996**, *37*, 4773.
(24) Takeuchi, H.; Okazaki, K. *Mol. Simul.* **1996**, *16*, 59−74.
(25) Chassapis, C. S.; Petrou, J. K.; Petropoulos, J. H.; Theodorou, D. N. *Macromolecules* **1996**, *29*, 3615−3624.
(26) Fukuda, M.; Kuwajima, *S. J. Chem. Phys.* **1997**, *107*, 2149−2158.
(27) Li, T.; Kildsig, D. O.; Park, K. *J. Controlled Release* **1997**, *48*, 57−66.
(28) Fritz, L.; Hofmann, D. *Polymer* **1997**, *38*, 1035.
(29) Bharadwaj, R. K.; Boyd, R. H. *Polymer* **1999**, *40*, 4229−4236.
(30) Cuthbert, T. R.; Wagner, N. J.; Paulaitis, M. E.; Murgia, G.; D'Aguanno, B. *Macromolecules* **1999**, *32*, 5017−5028.
(31) van der Vegt, N. F. A. *Macromolecules* **2000**, *33*, 3153−3160.
(32) Hofmann, D.; Fritz, L.; Ulbrich, J.; Schepers, C.; Böhning, M. *Polymer* **1996**, *37*, 4773−4785.
(33) Vineyard, G. H. *J. Phys. Chem. Solids* **1957**, *3*, 121−127.
(34) Arizzi, S. Diffusion of Small Molecules in Polymeric Glasses: A Modelling Approach. Ph.D. Thesis, MIT, 1990.
(35) Gusev, A. A.; Arizzi, S.; Suter, U. W.; Moll, D. J. *J. Chem. Phys.* **1993**, *99*, 2221−2227.
(36) Gusev, A. A.; Suter, U. W. *J. Chem. Phys.* **1993**, *99*, 2228−2234.
(37) Tsikoyiannis, J. G.; Wei, J. *Chem. Eng. Sci.* **1991**, *46*, 233−253.
(38) June, R. L.; Bell, A. T.; Theodorou, D. *N. J. Phys. Chem.* **1991**, *95*, 8866−8878.
(39) Snurr, R. Q.; Bell, A. T.; Theodorou, D. N. *J. Phys. Chem.* **1994**, *98*, 11948−11961.
(40) Greenfield, M. L.; Theodorou, D. N. *Mol. Simul.* **1997**, *19*, 329−361.
(41) Hofmann, D.; Fritz, L.; Ulbrich, J.; Paul, D. *Polymer* **1997**, *38*, 6145−6155.
(42) Greenfield, M. L.; Theodorou, D. N. *Macromolecules* **1998**, *31*, 7068−7090.
(43) Rallabandi, P. S.; Thompson, A. P.; Ford, D. M. *Macromolecules* **2000**, *33*, 3142−3152.
(44) Gusev, A. A.; Suter, U. W.; Moll, D. J. *Macromolecules* **1995**, *28*, 2582−2584.
(45) Weber, H.; Paul, W. *Phys. Rev. E* **1996**, *54*, 3999−4007.
(46) Amrani, S. E.; Kolb, M. *J. Chem. Phys.* **1994**, *98*, 1509−1513.
(47) Havlin, S.; Ben-Avraham, D. *Adv. Phys.* **1987**, *36*, 695−798.
(48) Haus, J. W.; Kehr, K. W. *Phys. Rep.* **1987**, *150*, 263−406.
(49) Greenfield, M. L.; Theodorou, D. N. *Macromolecules* **1993**, *26*, 5461−5472.
(50) McGreevy, R. L.; Howe, M. A. *Annu. Rev. Mater. Sci.* **1992**, *22*, 217−242.
(51) McGreevy, R. L.; Pusztai, L. *Mol. Simul.* **1988**, *1*, 359−367.
(52) Evans, D. J. *Mol. Simul.* **1990**, *4*, 409−411.
(53) Keen, D. A.; McGreevy, R. L. *Nature* **1990**, *344*, 423−425.
(54) Metropolis, N.; Rosenbluth, A. W.; Rosenbluth, M. N.; Teller, A. H.; Teller, E. *J. Chem. Phys.* **1953**, *21*, 1087−1092.
(55) Wolverton, C.; Zunger, A.; Schönfeld, B. *Solid State Commun.* **1997**, *101*, 519−523.
(56) This macrostate density was determined by counting the number of different sorption macrostates found in the six initial polymer structures in ref 42 and is much higher than that of methane-accessible clusters in Figure 3 of ref 49, showing that a penetrant interacting via a soft-sphere potential can probe more states than can a hard sphere, albeit at a significant energy cost.
(57) Rezac, M. E.; Pfromm, P. H.; Costello, L. M.; Koros, W. J. *Ind. Eng. Chem. Res.* **1993**, *32*, 1921−1926.
(58) Pfromm, P. H.; Koros, W. J. *Polymer* **1995**, *36*, 2379−2387.
(59) Greenfield, M. L. Molecular Modeling of Dilute Penetrant Gas Diffusion in a Glassy Polymer using Multidimensional Transition-State Theory. Ph.D. Thesis, University of California, Berkeley, 1996.
(60) Petropoulos, J. H. *J. Membr. Sci.* **1990**, *53*, 229−255.
(61) Allen, M. P.; Tildesley, D. J. *Computer Simulation of Liquids*; Oxford University Press: New York, 1987.
(62) Widom, B. *J. Chem. Phys.* **1963**, *39*, 2808−2812.
(63) Widom, B. *J. Phys. Chem.* **1982**, *86*, 869−872.
(64) Boone, T. D. Prediction of Glass-Melt Behavior and Penetrant Sorption Thermodynamics in Vinyl Polymers via Molecular Simulations. Ph.D. Thesis, University of California, Berkeley, 1995.
(65) Theodorou, D. N. In *Diffusion in Polymers*; Neogi, P., Ed.; Marcel Dekker: New York, 1996; pp 67−142.
(66) The macrostate-to-macrostate jump distance combines the distance traveled along a jump pathway with the distances traveled between each terminating local minimum and the center of the terminating sorption macrostate, as determined by geometric analysis. The distribution of distances between states was presented in Figure 11 of ref 42.
(67) Stauffer, D.; Aharony, A. *Introduction to Percolation Theory*, 2nd ed.; Taylor & Francis: London, 1992.
(68) de Gennes, P.-G. *La Recherche* **1976**, *7*, 919−927.
(69) Roman, H. E. *J. Stat. Phys.* **1990**, *58*, 375−382.
(70) Paetzold, O. *J. Stat. Phys.* **1990**, *61*, 495−500.
(71) Halperin, B. I.; Feng, S.; Sen, P. N. *Phys. Rev. Lett.* **1985**, *54*, 2391−2394.
(72) Feng, S.; Halperin, B. I.; Sen, P. N. *Phys. Rev. B* **1987**, *35*, 197−214.
(73) Kertész, J. *J. Phys., Lett.* **1981**, *42*, L393−L395.
(74) Elam, W. T.; Kerstein, A. R.; Rehr, J. J. *Phys. Rev. Lett.* **1984**, *52*, 1516−1519.
(75) Roberts, J. N.; Schwartz, L. M. *Phys. Rev. B* **1985**, *31*, 5990−5997.
(76) Pike, G. E.; Seager, C. H. *Phys. Rev. B* **1974**, *10*, 1421−1433.
(77) Seager, C. H.; Pike, G. E. *Phys. Rev. B* **1974**, *10*, 1435−1445.
(78) Kirkpatrick, S. *Rev. Mod. Phys.* **1973**, *45*, 574−588.
(79) Hunt, A. *J. Phys.: Condens. Matter* **1994**, *6*, 1239−1252.

(80) Karayiannis, N. C.; Mavrantzas, V. G.; Theodorou, D. N. *Chem. Eng. Sci.* **2001**, *56*, 2789−2801.
(81) Kehr, K. W.; Kutner, R. *Physica* **1982**, *110A*, 535−549.
(82) Brandrup, J.; Immergut, E. H.; Grulke, E. A. *Polymer Handbook*, 4th ed.; Wiley-Interscience: New York, 1999.
(83) van Krevelen, D. W. *Properties of Polymers*, 3rd ed.; Elsevier: Amsterdam, 1990.

MA002157H